Comparing Mfd- and UvrD-dependent models of transcription coupled DNA repair in live *Escherichia coli* using single-molecule tracking

Elżbieta Kaja[1,2]* , Donata Vijande[1],,Justyna Kowalczyk[1], Michał Michalak[1], Jacek Gapiński[1], Carolin Kobras[3], Philippa Rolfe[3] and Mathew Stracy[3]*

[1] Molecular Biophysics Division, Faculty of Physics, A. Mickiewicz University, Uniwersytetu Poznańskiego 2, 61-614 Poznan, Poland
[2] Department of Medical Chemistry and Laboratory Medicine, Poznań University of Medical Sciences, Rokietnicka 8, Poznań, Poland
[3] Sir William Dunn School of Pathology, University of Oxford, South Parks Road, Oxford OX1 3RE, UK

* To whom correspondence should be addressed, email: elzbieta.kaja@gmail.com and mathew.stracy@path.ox.ac.uk

Abstract

During transcription-coupled DNA repair (TCR) the detection of DNA damage and initiation of nucleotide excision repair (NER) is performed by translocating RNA polymerases (RNAP), which are arrested upon encountering bulky DNA lesions. Two opposing models of the subsequent steps of TCR in bacteria exist. In the first model, stalled RNAPs are removed from the damage site by recruitment of Mfd which dislodges RNAP by pushing it forwards before recruitment of UvrA and UvrB. In the second model, UvrD helicase backtracks RNAP from the lesion site. Recent studies have proposed that both UvrD and UvrA continuously associate with RNAP before damage occurs, which forms the primary damage sensor for NER. To test these two models of TCR in living *E. coli*, we applied super-resolution microscopy (PALM) combined with single particle tracking to directly measure the mobility and recruitment of Mfd, UvrD, UvrA, and UvrB to DNA during ultraviolet-induced DNA damage. The intracellular mobilities of NER proteins in the absence of DNA damage showed that most UvrA molecules could in principle be complexed with RNAP, however, this was not the case for UvrD. Upon DNA damage, Mfd recruitment to DNA was independent of the presence of UvrA, in agreement with its role upstream of this protein in the TCR pathway. In contrast, UvrD recruitment to DNA was strongly dependent on the presence of UvrA. Inhibiting transcription with rifampicin abolished Mfd DNA-recruitment following DNA damage, whereas significant UvrD, UvrA, and UvrB recruitment remained, consistent with a UvrD and UvrA performing their NER functions independently of transcribing RNAP. Together, although we find that up to ~8 UvrD-RNAP-UvrA complexes per cell could potentially form in the absence of DNA damage, our live-cell data is not consistent with this complex being the primary DNA damage sensor for NER.

Keywords

Nucleotide excision repair, Transcription coupled repair, UV-induced DNA damage, UvrD, Mfd

1. Introduction

Cells survive exposure to various external genotoxic factors, such as UV light or environmental toxins due to a set of DNA repair pathways working together and allowing these lesions to be repaired. Nucleotide excision repair (NER) in *E. coli* is performed by the UvrA, UvrB, UvrC and UvrD proteins to repair bulky, DNA helix-distorting lesions, such as the cyclobutane pyrimidine dimers (CPDs) that are formed by exposure to UV light. There are two subtypes of NER: Global genomic repair (GGR) and Transcription-coupled repair (TCR) (Fig. 1). Briefly, during GGR DNA lesions are located and repaired across the entire genome, whereas TCR acts on DNA damage only within sequences which are being actively transcribed. The GGR mechanism starts with UvrA proteins which search the entire genome for damage until a structural distortion is found and UvrB is recruited to verify the lesion [1,2]. UvrA then dissociates and UvrC is recruited to produce two incisions on both sides of the lesion, about 5 nt in the 3' direction and about 8 nt in the 5' direction. UvrD helicase is then recruited to displace the nicked single-stranded DNA fragment containing the distortion (approximately 14 nt) [3]. DNA polymerase I fills the gap from the free 3'OH end and the ligase seals the final nick [4].

The TCR pathway is initiated when the transcribing RNAP stalls upon encountering a DNA lesion. There are two differing models of the subsequent steps of TCR in bacteria; the 'Mfd model' and the 'UvrD model' (Fig. 1). In the Mfd model, stalled RNAPs are removed from the damage site by recruitment of the ATP-dependent translocase, Mfd. Mfd removes RNAP by pushing it forwards, terminating transcription in the process, which displaces the polymerase and exposes the lesion site to UvrA,B,C,D and NER proceeds as for GGR [5]. For a long time, Mfd was the only protein identified to remove stalled RNAP from the damage site [6–8]. Despite the important role that Mfd plays in TCR, deletion of Mfd in *E. coli* only leads to a modest increase in UV sensitivity [6,9,10]. Additionally, it has been argued that the relatively low processivity of Mfd could make Mfd-dependent TCR inefficient [11,12]. Therefore, it was hypothesized that there may be an alternative to Mfd to rescue these stalled polymerases.

In 2014, the involvement of UvrD in TCR as an alternative to Mfd was identified [13]. UvrD helicase is involved in many cellular processes in *E. coli*, including NER, mismatch repair, DNA replication and recombination. The best studied function of UvrD is displacement of the damaged DNA fragment during NER following the action of UvrC. In the 'UvrD model' of TCR, UvrD also acts as an RNAP backtracking factor which pushes the polymerase backwards exposing the damaged site to be repaired by other proteins. Unlike the Mfd pathway, after the repair is complete, the backtracked polymerase can continue transcription without losing the nascent mRNA. It was originally hypothesised that UvrD-dependent TCR occurs particularly during high-levels of DNA damage [14]. Recent studies have proposed that both UvrD, together with UvrA and NusA, continuously associate with RNAP forming a surveillance pre-TCR complex which scans DNA for damage [15]. Upon RNAP stalling in response to DNA damage the pre-TCR complex recruits a second UvrD monomer to create a functional helicase which pushes RNAP backwards to expose the DNA lesion. NER is then initiated by recruiting a second UvrA and UvrB to the stalled RNAP-UvrA-UvrD-NusA pre-TCR complex.

Moreover, a study from the same group suggested that TCR is not a minor sub-pathway of NER, but accounts for the vast majority of chromosomal repair events and dominates over GGR [16]. In our previous work, we showed that NER initiation involves a two-step mechanism in which UvrA scans the genome and locates DNA damage independently of UvrB, in contrast to the earlier models in which a $UvrA_2UvrB_2$ complex is the initiating factor [1] While this work did not focus on TCR, we note our previously proposed model of NER initiation is consistent with the recently proposed pre-TCR complex being the primary damage sensor initiating NER since this complex contains UvrA but not UvrB. However, other studies using different *in vitro* and *in vivo* methods have concluded that Mfd remains the only protein necessary for TCR [9,17–19]. The relative involvement of Mfd, UvrD, and UvrA in TCR, in both the presence and absence of DNA damage, therefore warrants further study.

Here, we directly compare the behaviour of UvrD, Mfd, UvrA, UvrB and RNAP in living *E. coli* before and after UV exposure using photoactivated localisation microscopy (PALM) combined with single particle tracking [1]. By analysing the abundance and intracellular mobility of these proteins, we determined the number of proteins that could be present together in complexes in the absence of DNA damage. Furthermore, we determine the proportion of molecules recruited to DNA following UV-induced DNA damage. We observed differences in the level of recruitment to DNA and binding times between Mfd and UvrD following UV exposure. In contrast to Mfd, recruitment of UvrD to DNA damage remained even when transcription was inhibited, and was completely dependent on the presence of UvrA, consistent with it performing is NER function independently of transcribing RNAP. Together, although we find that up to ~8 UvrD-RNAP-UvrA complexes per cell could potentially form in the absence of DNA damage, our live-cell data was not consistent with this complex being the primary DNA damage sensor for NER.

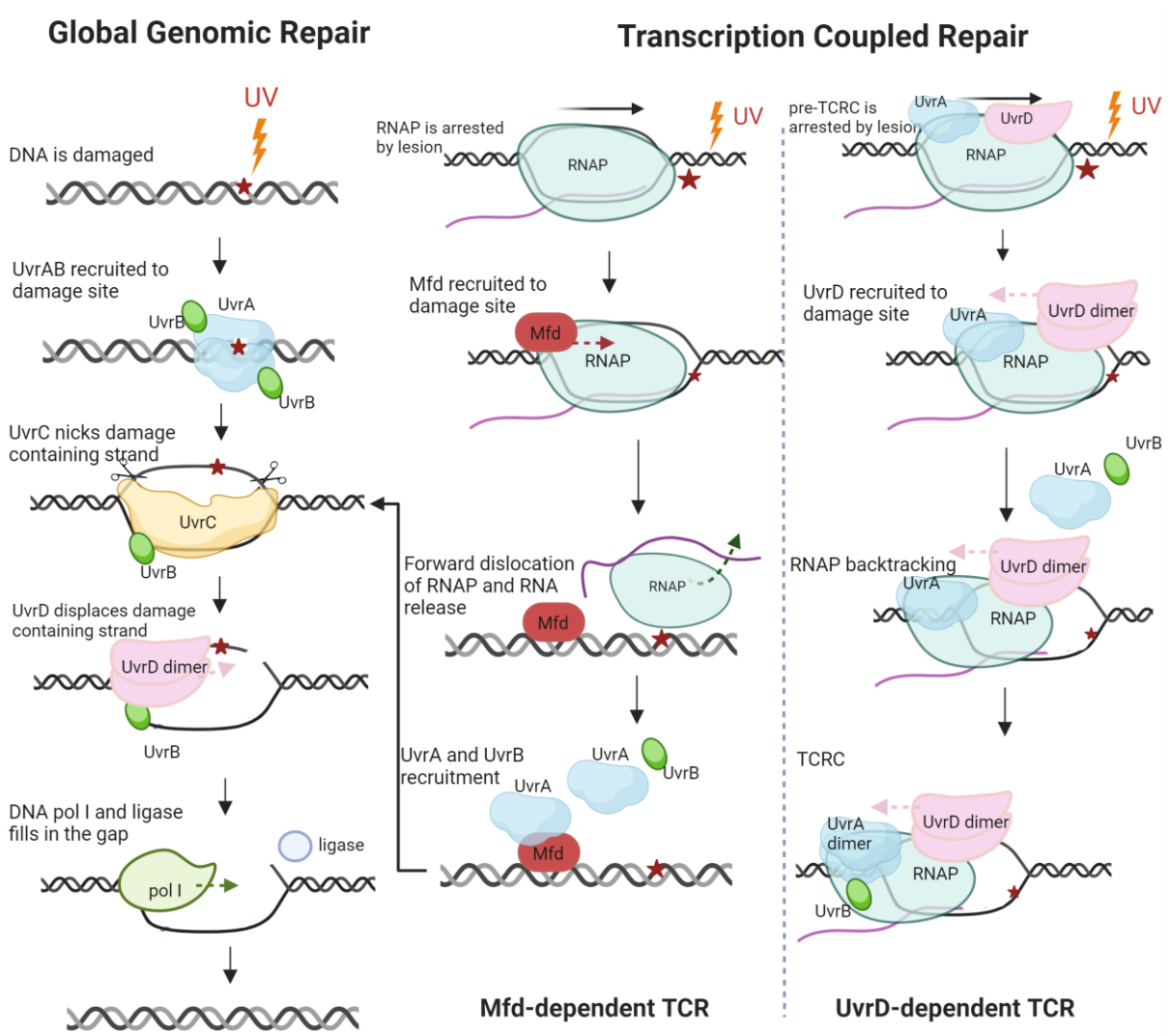

Figure 1. Nucleotide excision repair (NER) pathways. *The NER pathway can be divided into two subtypes: global genomic repair (GGR) and transcription coupled repair (TCR). Two different models for TCR exist: In the Mfd-dependent model, RNAP stalling at DNA lesions leads to recruitment of Mfd, which removes RNAP by pushing it forwards. Mfd subsequently recruits UvrA and UvrB to DNA, and NER proceeds as for GGR. In the UvrD-dependent model, UvrD and UvrA continuously associate with RNAP forming a surveillance pre-TCR complex which scans DNA for damage. Upon RNAP stalling at a DNA lesion the pre-TCR complex recruits a second UvrD monomer to create a functional helicase which pushes the polymerase backwards exposing the damaged site. NER is then initiated by recruiting a second UvrA and UvrB to the TCR complex.*

2. Materials and methods

Bacterial strains

All bacterial strains used were derivatives of *E. coli* K-12 AB11572 [20] except for rpoC-PAmCherry which is a derivative of K-12 MG1655. All strains used in this study are listed in Supplementary table 1. Replacement of endogenous genes with C-terminal fusions with the photoactivatable fluorescent protein, PAmCherry [21] were performed using Lambda red recombination [22] and fusion genes were moved to the final strains by P1 phage transduction [23].

The flexible 11 amino acid linker (SAGSAAGSGEF) was introduced between full length of each protein and PAmCherry protein. The oligonucleotides used to make the strains are shown in Supplementary Table 2. All deletions were introduced *de novo*. The first and last 50 bp of coding sequence was left in order to prevent removal of potential regulatory elements for other genes. For multiple insertions of modified genes, the *kan*^{r} gene was removed using site-specific recombination through expression of the Flp recombinase from plasmid pCP20. Correct insertion of the fragment into the chromosome was evaluated by PCR using primers flanking the insertion site. Strains carrying UvrD or Mfd PAmCherry fusions expressed from their endogenous promoter showed no increase in the sensitivity to UV compare to AB1157 wild-type (Supplementary figure 1). UvrA-PAmCherry and UvrB-PAmCherry similarly showed no increase in UV sensitivity as detailed in Stracy et al 2016.

UV sensitivity assay

For UV sensitivity assays, 50 µl of overnight culture was diluted into 5 ml of fresh LB media and grown for 2 h at 37 °C with shaking (220 rpm). The OD_{600} was measured and adjusted to be consistent between the different strains. The culture was serial diluted in 10-fold steps and 10 µl of each dilution plated in triplicate on LB agar plates. Each plate was exposed to 254 nm UV (neoLab, UV lamp, Type 6) for three different UV doses: 0, 10 and 20 J/m^2). Plates were incubated at 37 °C overnight and the number of colonies counted. At least three independent experiments were performed for each strain. The mean percentage survival was plotted as a function of UV dose (Supplementary figure 1).

Microscopy sample preparation

Strains were streaked onto Luria–Bertani plates with appropriate antibiotics. Single colonies were inoculated into M9 glycerol (0.2%) and grown overnight at 37 °C to A600 0.4–0.6, then diluted into fresh M9 and grown to A600 of 0.1. Before imaging, 1 ml of the culture was spun down in a 1.5 ml microcentrifuge tube for 1 min at 5,000 rpm. 950 µl of the supernatant was discarded and the cells resuspended in the remaining 50 µl. 1 µl of the cells was placed on a freshly prepared 1% low fluorescence agarose (Bio-Rad) pad and covered with a coverslip.

Equal parts of 2 x M9 Glycerol and melted 2% agarose were mixed and a droplet placed between two coverslips to make 1% agarose pads and allowed to set for 1 h before adding cells for imaging. Coverslips used for imaging were cleaned in a plasma cleaner to remove background fluorescence. The UV damage in short-exposure PALM was induced by exposure of the bacterial cells placed on the agarose pad to UV light (50 J/m^2). Cells were imaged between 5 and 20 minutes after the exposure. Where indicated, rifampicin (Rif) was added to bacterial culture in M9 to a final concentration of 100 µg/ml for 30 min prior to imaging.

For photobleaching controls using fixed cells, centrifuged cells were resuspended into 2.5% paraformaldehyde in M9 media and fixed for 45 min shaking at 22ºC. Fixed cells were washed, then immobilized on agarose pads as for live cells.

PALM microscopy

Live cell photoactivated single-molecule tracking was performed on a custom-built total internal reflection fluorescence (TIRF) microscope built around the Rapid Automated Modular Microscope (RAMM) System (ASI Imaging) as previously described [1,24]. PAmCherry activation was controlled by a 405 nm laser and excited with 561 nm. All lasers were provided by a multi-laser engine (iChrome MLE, Toptica). At the fiber output, the laser beams were collimated and focused (100x oil immersion objective, NA 1.4, Olympus) onto the sample under an angle allowing for highly inclined thin illumination (Tokunaga et al., 2008). Fluorescence emission was filtered by a dichroic mirror and filter (ZT405/488/561rpc & ZET405/488/561NF, Chroma). PAmCherry emission was projected onto an EMCCD camera (iXon Ultra, 512x512 pixels, Andor). The pixel size was 96 nm. Transmission illumination was provided by an LED source and condenser (ASI Imaging and Olympus). Sample position and focus were controlled with a motorized piezo stage, a z-motor objective mount, and autofocus system (MS-2000, PZ-2000FT, CRISP, ASI Imaging). Movies of 10,000 frames at 23ºC were acquired under continuous 561 nm laser excitation at 250 W/cm^2 with an exposure time of 15 ms. Camera readout was 0.48 ms giving frame intervals of 15.48 ms.

Localization and tracking

Single-molecule-tracking analysis was performed using custom-written MATLAB software (MathWorks): fluorophore images were identified for localization by band-pass filtering and applying an intensity threshold to each frame of the movie [1]. Candidate positions were used as initial guesses in a two-dimensional elliptical Gaussian fit for high-precision localization. Free fit parameters were x-position, y-position, x-width, y-width, elliptical rotation angle, intensity, background. Localizations were segmented based on cell outlines obtained from MicrobeTracker applied to the brightfield snapshots. Single-particle tracking analysis was performed by adapting the MATLAB implementation of the algorithm described in [26]. Positions were linked to a track if they appeared in consecutive frames within a window of 5 pixels (0.48 μm). When multiple localizations fell within the tracking window, tracks were linked such that the sum of step distances was minimized. We used a 'memory' parameter of 1 frame to allow for transient disappearance of the fluorophore within a track due to blinking or missed localization.

Measuring the diffusion of tracked molecules

We determined the mobility of each molecule by calculating an individual apparent diffusion coefficient, D_i^*, from the one-step mean-squared displacement (MSD) of the track using:

$$D_i^* = \frac{1}{4n\Delta t}\sum_{i=1}^{n}[x(i\Delta t) - x(i\Delta t + \Delta t)]^2 + [y(i\Delta t) - y(i\Delta t + \Delta t)]^2$$

Where $x(t)$ and $y(t)$ are the coordinates of the molecule at time t, the frame time of the camera is Δt, and n is the number of frames over which the molecule is tracked. For a molecule diffusing with an

apparent diffusion coefficient D^*, the probability of measuring a D_i^* by tracking it over n frames, is given by [26]:

$$p(D_i^*) = \frac{1}{(n-1)!} * \left(\frac{n}{D}\right)^n * (D_i^*)^{n-1} * exp\left(\frac{-nD_i^*}{D}\right)$$

In order to determine the apparent diffusion coefficient, D^*, from the population of individual single-molecule D_i^* values, longer tracks were truncated after 5th localization (i.e. $n = 4$). The D_i^* distribution was then fitted with the equation for $n = 4$:

$$p(D_i^*) = \frac{1}{6} * \left(\frac{4}{D}\right)^4 * (D_i^*)^3 * exp\left(\frac{-4D_i^*}{D}\right)$$

Fits were performed using maximum likelihood estimation in MATLAB. For unperturbed cells the protein diffusion distributions were fit with a model containing two molecular species with diffusion coefficients D_1^* and D_2^*: representing immobile molecules bound to DNA for the entire trajectory, and mobile molecules diffusing and binding only transiently to DNA:

$$p(D_i^*) = \left[\frac{A_1}{6} * \left(\frac{4}{D_1^*}\right)^4 * (D_i^*)^3 * exp\left(\frac{-4D_i^*}{D_1^*}\right)\right] + \left[\frac{(1-A)}{6} * \left(\frac{4}{D_2^*}\right)^4 * (D_i^*)^3 * exp\left(\frac{-4D_i^*}{D_2^*}\right)\right]$$

where $A$and $1 - A$ are the fraction of molecules found in each state. The localization uncertainty, σ_{loc}, manifests itself as a positive offset of $\sigma_{loc}^2/\Delta t$ in the D^* value [27]. Based on the estimated localization uncertainty of ~38 nm for our measurements, we expected a positive shift in the mean D^* value of immobile molecules to ~0.1 $\mu m^2 s^{-1}$. To plot maps of tracks from mobile and immobile molecules, we used a threshold of 0.1 $\mu m^2 s^{-1}$ to separate the populations and to constrain the D_1^* value when fitting the two species model to the data. Where indicated error bars represent the standard error of the mean from the results of independently fitting at least three experimental repeats. Statistical significance testing is by Student's *t*-test.

Molecule counting

We counted the total number of Mfd or UvrD molecules by recording 30,000 frames until no further activation was observed. Cells were segmented from transmission images using MicrobeTracker [25]. Localizations within cell boundaries were tracked and the number of tracked molecules per cell established. We note that the copy numbers presented here may be underestimates of the true copy numbers, since only 49% of PAmCherry were shown to be photoactivatable in studies in eukaryotic cells [28]. However, the ratio between copy numbers of the different proteins in this study is not affected by this potential underestimation as all proteins are PAmCherry fusions measured under the same conditions.

Measuring Long-lasting Binding Events

Long duration binding events were measured and corrected for photobleaching following previously described methodology [26]. PALM movies to measure long duration binding events 500 frames were recorded per field of view at low continuous 561-nm excitation intensities using long exposure times (1 s/frame). To minimise the influence of photobleaching on the apparent binding times, 561 nm laser excitation at 5 W/cm2 was used. At these exposure times mobile UvrD-PAmCherry and Mfd-PAmCherry molecules are motion blurred over a large fraction of the cell, whereas immobile molecules still appear as point sources, producing a diffraction limited spot. Elliptical Gaussian fitting was used as described earlier. Bound and mobile molecules were distinguished by the width of the elliptical fits, with thresholds short axis-width < 160 nm and long axis-width < 200 nm to identify bound molecules. The probability of observing a particular on-time is the product of the underlying binding-time probability and the bleaching probability. The bleaching-time distributions were measured independently using UvrD-PAmCherry in cells fixed with paraformaldehyde, with the same acquisition and excitation conditions. On-time and bleaching-time distributions were fitted with single-exponential functions to extract exponential-time constants t_{on} and t_{bleach}, and the binding-time constant was calculated by $t_{bound} = t_{on} \cdot t_{bleach} / (t_{bleach} - t_{on})$. Stochastic photoactivation of UvrD-PAmCherry and Mfd-PAmCherry molecules before or during binding events does not influence our measurement, because the observed binding times follow an exponential distribution and are therefore memoryless.

3. Results

Single molecule tracking of TCR proteins

To better understand the behaviour of UvrA, UvrB, UvrD, and Mfd during DNA damage repair and determine their relative involvement in RNAP binding during TCR we used PALM combined with single-particle tracking. To be able to image and track these proteins inside living cells, we constructed strains with C-terminal fusions of UvrD and Mfd with the photoactivatable fluorescent protein PAmCherry (Supplementary table 1). To verify that these fusions were fully functional we measured cell survival following UV exposure. Deletion of *uvrD* is known to lead to an extremely UV sensitive phenotype [29] . In agreement with this, a *ΔuvrD* strain, showed no survival even at the lowest UV dose (10 J/m^2). A *Δmfd* mutant showed a modest sensitivity to UV (about 10% lower survival after 10 and 20 J/m^2 UV dose), confirming the results of others [6,9,10]. Both the UvrD-PAmCherry and Mfd-PAmCherry strains showed the same survival as wildtype following UV exposure, confirming the functionality of these fusions in performing NER (Supplementary figure 1). We also included previously constructed PAmCherry fusion strain of UvrA and UvrB, both of which also showed the same survival as wildtype following UV exposure [30]. We further include a PAmCherry fusion to the beta' subunit of RNAP, rpoC-PAmCherry [30].

To measure the mobility of these NER and TCR proteins in live *E. coli*, we performed PALM microscopy. Sparse photoactivation of PAmCherry with 15 ms exposure allowed us to track the

movements of photoactivated molecules by linking together localisations from individual molecules into trajectories (Fig. 2A). Following the same approach previously used for other NER proteins and various other DNA-binding proteins [1,31], we calculated an apparent diffusion coefficient (D*) value for each trajectory to distinguish DNA-bound populations of molecules from mobile molecules searching for substrates (Fig. 2B; Supplementary table 3). To this end, we fitted the histogram of D* values for individual UvrD and Mfd trajectories with a two species model representing an immobile population bound directly or indirectly to DNA ($D^*=0.1\ \mu m^2\ s^{-1}$) and a mobile population representing molecules diffusing and searching for lesions and not engaged in NER at the moment of measurement [1,31].

For UvrD we observed that a relatively small fraction of molecules appears to be DNA-bound in living cells in the normal growth conditions (10.3 ± 0.7 %; errors indicate s.e.m from fitting to at least three experimental repeats; Table 1) with most molecules diffusing and searching for substrate (Table 1;Fig. 2C,D). Exposure to 50 J/m^2 UV lead to a significant increase in the proportion of DNA-bound molecules (24.2 ± 2.3 %, p=0.003), which we attribute to molecules recruited to DNA and involved in repairing DNA damage or removing stalled RNAP (Table 1; Fig. 2E,F). In the case of Mfd, UV exposure led to a much higher percentage of molecules recruited to DNA, from 18.9 ± 1.3 % to 68.0 ± 2.8 % (p=0.003; Table 1; Fig. 2G,H; Fig. 4B). The increase in immobile molecules can be observed in cells overlaid with measured Mfd trajectories (Fig. 2I,J). UvrA DNA binding increased from 32.0 ± 2.2 % to 65.4 ± 2.8 % following 50 J/m^2 UV and UvrB DNA binding increased from 17.0 ± 0.5 % to 50.1 ± 4.0 % following exposure, in agreement with our previous observations [1]. 33.8 ± 2.5 % of RNAP are DNA bound at any given time under the growth conditions used, and this fraction is not significantly affected by exposure to UV. Although the overall fraction of RNAP bound to DNA changes little following UV exposure, some proportion of elongating RNAP will become stalled, but these cannot be distinguished with our assay. We note that increased DNA-binding due to RNAP stalling at lesions may be counterbalanced by the effect of stalled RNAP inhibition active transcription on the same operon.

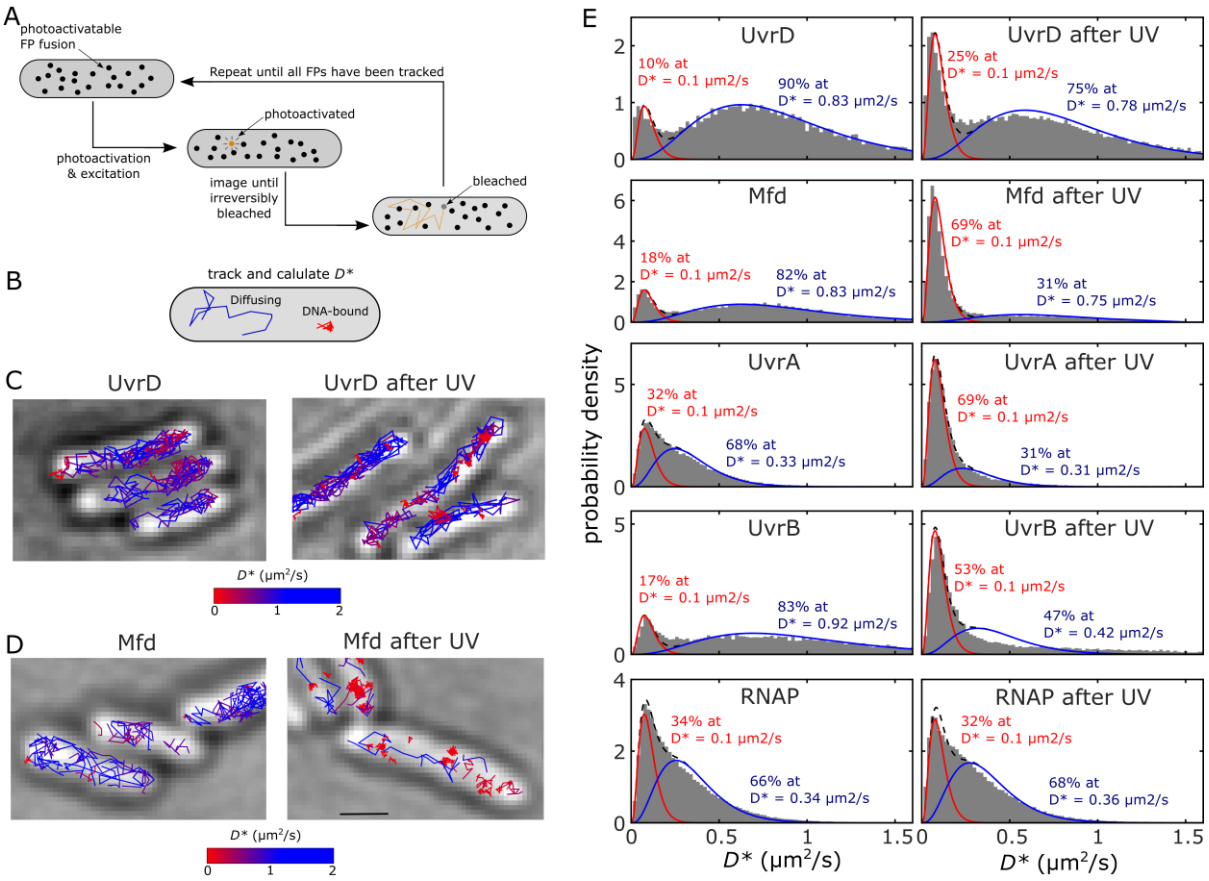

Figure 2. Live-cell single-molecule imaging of TCR protein recruitment to DNA damage. *A) Cartoon showing the process of photoactivated localisation microscopy combined with single-particle tracking. B) Cartoon showing how an apparent diffusion coefficient (D*) can be calculated from protein trajectories and the D* value used to distinguish immobile DNA-bound molecules from diffusion molecules. C) Example cells showing UvrD-PAmCherry trajectories coloured according to their measured mobility during unperturbed growth conditions (left) and following exposure to 50 J/m2 UV (right). D) Example cells showing Mfd-PAmCherry trajectories coloured according to their measured mobility during unperturbed growth conditions (left) and following UV exposure (right). E) Histograms of single-molecule D* values from tracked PAmCherry fusions to different proteins involved in TCR before (left) and after (right) UV exposure. Histograms are fitted to a two species model; an immobile population, representing molecules directly or indirectly bound to DNA (constrained fit at D=0.1 μm² s⁻¹), and mobile population, representing molecules diffusing and searching for lesions. Number of trajectories represented in each histogram: UvrD = 15,745; UvrD UV = 21,168; Mfd = 18,720; Mfd UV = 27,804; UvrA = 32,100; UvrA UV = 19,548; UvrB = 14,339; UvrB UV = 15,936; RNAP = 120,546; RNAP UV = 61,119. Histograms represent the pooled data from all experimental repeats; mean values and errors from the s.e.m from individually fitting to each experimental repeats are shown in Table 1.*

Determining the number of complexed molecules in the absence of DNA damage.

A key difference between the two models of TCR, is the formation of a pre-TCR complex in which a UvrA monomer and UvrD monomer continuously associate with RNAP in the absence of DNA damage. In contrast, in the Mfd model, Mfd is recruited to RNAP only after DNA damage occurs leading to RNAP stalling. UvrA and UvrD perform the function in damage recognition and strand displacement downstream of this step. To compare these models, we sought to determine if UvrA-UvrD-RNAP complexes are present in the absence of DNA damage by comparing protein copy numbers and their distribution of D* values (Fig. 3).

To determine the number of proteins per cell we imaged using PALM until no further photoactivation of PAmCherry was observed. Cells were segmented based on brightfield images and individual molecules were tracked and the total number of molecules were counted for each cell. Our data showed that the mean copy number of UvrD and Mfd molecules in normal conditions is 80 ± 10 and 131 ± 16 molecules per cell, respectively (Fig. 3B), which is consistent with the numbers collected in the Protein Abundance Database (PaxDB) database (pax-db.org, accession date: 12/01/2023) [32]. In our previous work we measured the copy number of UvrA and UvrB under the same growth conditions as 84 ± 12 and 88 ± 17, respectively. UvrA, UvrB and UvrD are therefore present in the cell at close to equimolar concentrations. RNAP, in contrast, is present at 2,710±700 copies per cell [13,30,32–34]. Our data shows that the mobility of RNAP and UvrA are very similar before DNA damage, consistent with UvrA being potentially forming complexes with to RNAP (Fig. 3A). However, this was not the case for UvrD, which showed a much smaller proportion of immobile molecules and a much faster diffusing mobile population. Since UvrA and UvrD are present at equimolar concentrations, their very different intracellular mobilities are therefore not consistent with a large proportion of these proteins being complexed in putative pre-TCR complexes in the absence of damage. Similarly, the mobility of UvrB shows that most UvrB are not complexed with UvrA in solution, as we report previously [1]. This was also the case for Mfd, consistent with this enzyme being recruited to RNAP after DNA damage occurs (Fig. 3A). Since the pre-TCR complexes are expected to be formed on elongating RNAP we further determined the number of molecules that could be associated with DNA or DNA-bound RNAP based on the protein copy number and fraction of DNA-bound molecules (Table 1). In the absence of DNA damage, 27 ± 5 UvrA molecules per cell are immobile and therefore could in principle be associated with DNA-bound RNAP. For UvrD, however, only 8 ± 3 molecules per cell are DNA-bound in the absence of DNA damage. Therefore, only up to ~8 DNA-bound UvrD-RNAP-UvrA complexes per cell could potentially be present at any given time in the absence of DNA damage.

Determining the number of molecules recruited to DNA lesions

Based on their copy numbers we estimate that on average the number of UvrD bound to DNA increases from 8 ± 3 molecules per cell under normal growth conditions to 19 ± 4 molecules following exposure to 50 J/m^2 UV (Table 1). For Mfd the number of DNA-bound enzymes increases from 24 ± 5 to 89 ± 5 molecules following UV exposure. Next, we measured the dwell time on DNA for UvrD, UvrA and Mfd to provide a better understanding of their activity before and during DNA damage repair. In both models of TCR most Mfd is expected to be recruited following RNAP stalling and long-lived binding would therefore be expected primarily after UV exposure. In contrast, UvrA and UvrD would be expected to have long dwell times in the absence of DNA damage if they form long-lived UvrD-RNAP-UvrA DNA-bound pre-TCR complexes in the UvrD model of TCR. We measured the DNA binding times using 1 s exposure time and corrected for photobleaching by measuring an observed binding time in fixed cells (see Methods) [1]. The binding time of UvrD and Mfd in unperturbed cells

was 1.3 s and 2.7 s, respectively. The binding time of UvrA was 2.2 s in unperturbed cells, consistent with our previously published measurements for this protein using the same methodology (Fig. 3C) [1]. In the absence of DNA damage these dwell times do not indicate that UvrD and UvrA molecules form particularly long-lived DNA-bound complexes. The observed Mfd binding time similarly suggest that most binding events do not represent long-lived association with RNAP, which have been reported by others to occur in the absence of DNA damage with a duration of 18 s [35].

Following UV exposure, the binding time of Mfd increased from 2.7 s to 10.7 s, which is consistent with previous studies suggesting that Mfd takes over ten seconds on average to displace the stalled RNAPs from damage sites [11,12,35]. Our result show that average Mfd dwell times on DNA is significantly increased following UV exposure, consistent with a change in activity, likely reflecting more abortive binding events in the absence of damage and more molecules engaged in complete RNAP binding and removal following UV exposure. The binding time of UvrD also increases following UV exposure, but more modestly, from 1.3 s under normal conditions, to 2.8 s after UV exposure (Fig. 3C). This difference in binding times for these two enzymes is consistent with previous studies showing that UvrD is a “fast” helicase requiring only about 1.5 s to remove DNA fragment during NER [36], whereas the action of Mfd is considered slower [14]. The binding time of UvrA increased from 2.2 s to 14 s following UV exposure, consistent with our previous report [1].

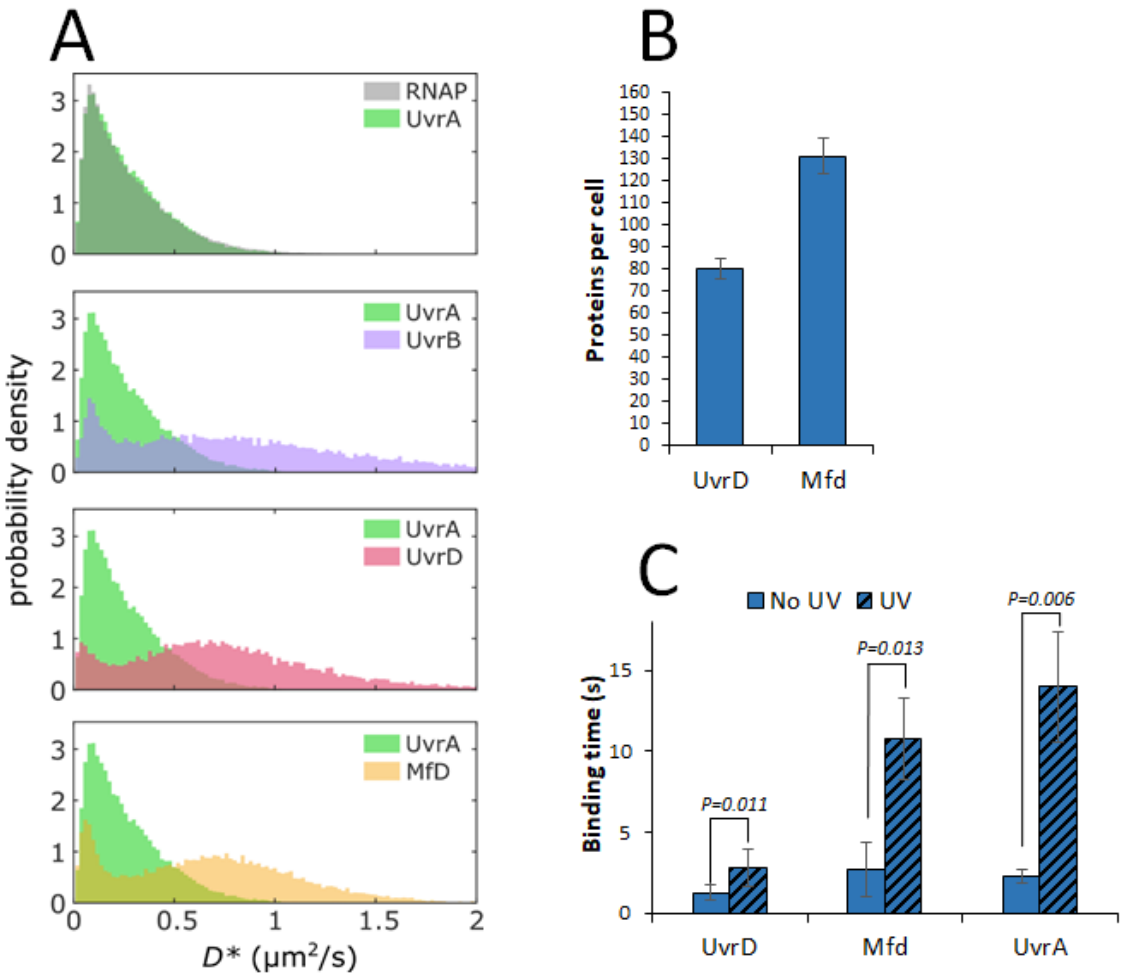

368
369

370 ***Figure 3. Determining the number of potentially complexed molecules.*** *(A) The histogram of single-molecule*
371 *D* values from tracked UvrA-PAmCherry in unperturbed cell overlaid on the histogram of other TCR proteins. (B)*
372 *Mean copy numbers for UvrD and Mfd monomers calculated in >500 cells growing in unperturbed conditions.*
373 *Error bars indicate s.e.m. of three experimental repeats. (B) Binding time distributions for UvrD, Mfd and UvrA*
374 *before and after UV exposures after correction for photobleaching. Binding times were measured with 1 s*
375 *exposures. The average binding time for UvrD increased from 1.27 s to 2.81 s, for Mfd increased from 2.67 s to*
376 *10.73 s and for UvrA increased from 2.22 s to 13.97 s after UV exposure. Error bars indicate s.e.m. of three*
377 *experimental repeats. Statistical significance calculated using Student's t-test.*

378

Table 1. TCR proteins' DNA binding and mobility before and after UV exposure

Protein	Copy number	Average % of molecules DNA bound	Average apparent diffusion coefficient of mobile population ($\mu m^2/s$)	Number of molecules bound to DNA (directly or indirectly via RNAP)	Average % of molecules DNA bound	Average apparent diffusion coefficient of mobile population ($\mu m^2/s$)	Estimated number molecules bound to DNA (directly or indirectly via RNAP)
		Before UV exposure			After UV exposure		
RNAP	2,710±700*	33.8 ± 2.5	0.34 ± 0.02	916 ± 304	32.2 ± 2.8	0.34 ± 0.05	872 ± 301
UvrA	84 ± 12†	32 ± 2.2	0.31 ± 0.02	27 ± 5	65.4 ± 2.8	0.29 ± 0.04	54 ± 10
UvrB	88±17†	17 ± 0.5	0.90 ± 0.06	15 ± 3	50.1 ± 4.0	0.42 ± 0.22	44 ± 12
UvrD	80 ± 10	10.3 ± 0.7	0.71 ± 0.01	8 ± 3	24.2 ± 2.3	0.71 ± 0.01	19 ± 4
Mfd	131 ± 16	18.9 ± 1.3	0.79 ± 0.03	24 ± 5	68.0 ± 2.8	0.74 ± 0.03	89 ± 5

†Copy numbers measured in Stracy et al 2016. *Copy number measured in Stracy et al 2015. The reported percentage of DNA-bound molecules and apparent diffusion coefficients represent the mean and s.e.m of the values extracted from individually fitting the histogram of *D** values from at least three experimental repeats. The number of DNA-bound molecules is calculated from the copy number multiplied by the fraction of DNA-bound molecules with propagation of the respective errors. Note, the histograms and fitted values in Fig. 2 represent the pooled data from all experimental repeats.

UvrD and Mfd do not compete for stalled-RNAP removal.

The best studied function of UvrD during NER is displacement of the damaged DNA fragment following the recognition of DNA lesions by UvrA and UvrB and strand nicking by UvrC. In the UvrD model of TCR, UvrD also acts upstream in the pathway by backtracking stalled RNAP[13]. To determine where in the NER pathway recruitment of UvrD to DNA was occurring we constructed UvrD-PAmCherry strain with UvrA deleted. Importantly, no significant increase in the fraction of DNA-bound UvrD molecules following UV exposure was seen in a *ΔuvrA* background (p=0.3). This observation fits with the GGR and the Mfd models of TCR, where the action of UvrD is strand displacement occurring downstream from the action of UvrA (Fig. 4A). Since the UvrD model of TCR involves a recognition complex of UvrA-RNAP-UvrD, an alternative explanation could be that when UvrA is absent from the pre-TCR complex, recruitment of subsequent UvrD upon RNAP stalling no longer occurs.

In the Mfd model of TCR, Mfd binding to stalled RNAP promotes subsequent recruitment of UvrA. In contrast, in a recent study describing the UvrA-RNAP-UvrD pre-TCR complex Mfd recruitment to RNAP was found to be strongly dependent on UvrA. This was interpreted as the UvrA-containing TCR complex acting to recruit Mfd, rather than the other way around. To test this, we measured Mfd in a *ΔuvrA* background. In our assay we found that Mfd recruitment to DNA following

UV exposure is unaffected by the absence of UvrA, in agreement with the upstream role of this protein in the Mfd model of TCR and contrast to the recent evidence suggesting the UvrA-RNAP-UvrD pre-TCR recruits Mfd (Fig. 4B).

If Mfd and UvrD both compete for binding of stalled RNAP, the absence of the competitor would be expected to increase the percentage of immobile molecules following UV exposure due to the increased availability of stalled-RNAP. Mfd cannot act as a replacement for UvrD in its other roles during DNA damage repair, such as displacement of the damaged-strand following DNA nicking by UvrC. We therefore constructed UvrD-PAmCherry and Mfd-PAmCherry strains with the respective competitor protein deleted. We found that in both cases deletion of the competitor did not affect the level of recruitment of molecules to DNA (Fig. 4A,B), suggesting that these proteins are not significantly competing for the same substrate, i.e. stalled RNAP.

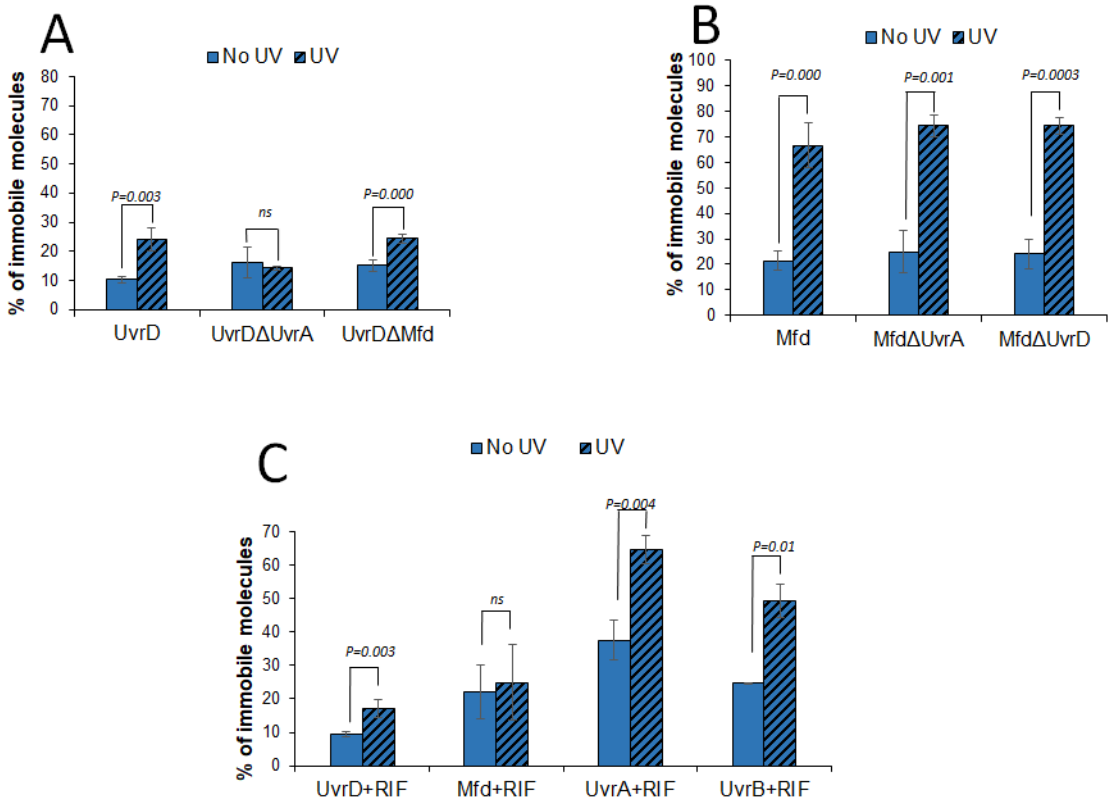

Figure 4. UvrD and Mfd do not compete for stalled-RNAP removal. *(A) Percentage of immobile UvrD molecules extracted by fitting two species model to the UvrD D* distribution before and after exposure to UV in WT cells, ΔuvrA and, Δmfd. (B) Percentage of immobile Mfd molecules extracted by fitting two species model to the Mfd D* distribution before and after exposure to UV in WT cells, ΔuvrA and ΔuvrD. (C) Fractions of immobile UvrD and Mfd molecules extracted by fitting two species model to the UvrD, Mfd, UvrA and UvrB D* distributions before and after exposure to UV in rifampicin treated cells. Error bars represent s.e.m from the results of independently fitting at least three experimental repeats. Statistical significance testing calculated by Student's t-test.*

UvrA and UvrD recruitment to DNA is independent of RNAP activity

We then tested if the UvrD and Mfd behaviours are dependent on RNAP activity. To block active transcription, we used rifampicin (Rif), an antibiotic, which binds to the β subunit of RNAP and prevents RNAP entering into transcription elongation. It was shown that a very high concentration of Rif before the UV exposure almost completely abolished CPD removal during *E.coli* recovery [15] suggesting the importance of RNAP activity in NER [11]. In the Mfd-model of TCR Rif treatment would be expected to strongly inhibit UV-induced DNA recruitment of Mfd, but ongoing GGR would still allow UvrA, UvrB and UvrD DNA recruitment. In contrast, in the UvrD-dependent model, UvrD recruitment to DNA lesions would also be expected to be inhibited by Rif. Furthermore, since it is proposed that UvrA-RNAP-UvrD complexes are the main damage sensor, universal inhibition of UV-induced DNA recruitment for all NER proteins would be expected.

No significant increase in the DNA-bound fraction of Mfd was observed after UV exposure in Rif treated cells (100 µg/ml for 30 min), showing that recruitment of Mfd to DNA is indeed dependent on active transcription as expected for both models of TCR. However, a lowered but significant increase in UV induced DNA-recruitment of UvrD was still observed in Rif treated cells (Fig. 4C; Fig. S2). Since UvrD is also involved mismatch repair, it was possible that the increase in DNA binding following UV exposure in Rif treated cells could have been UvrD involved in mismatch repair. Indeed, using a MutS-PAmCherry fusion to report on the initiation of mismatch repair, showed that MutS is still recruited to DNA following UV exposure in Rif treated cells (Fig. S2). To verify that UvrD DNA recruitment during Rif treatment is not only a consequence of its involvement in mismatch repair we tested UvrD-PAmCherry in a *ΔmutL* background. The *mutL* deletion did not affect the UV-induced DNA recruitment of UvrD in Rif treated cells (Fig. S2). We also found that significant UV-induced DNA recruitment of UvrA and UvrB was also still observed in Rif treated cells (Fig. 4C). At the concentrations tested, Rif treatment therefore selectively abolishes UV-induced DNA recruitment of Mfd, but significant DNA recruitment of UvrD, UvrA and UvrB remains.

4. Discussion

There are two proposed pathways of TCR in bacteria: a Mfd-dependent pathway and a UvrD-dependent pathway, with contradictory results in the literature arguing for and against the relative importance of these two models. The Sancar group have presented results showing that Mfd is the only protein involved in RNAP displacement during TCR. First, they used an *in vitro* repair synthesis assay to observe that an Mfd deficient strain is incapable of strand-specific repair [9]. Then, they used genome-wide excision repair–sequencing (XR-seq) and confirmed their previous results. By isolating and sequencing specifically CPD containing DNA fragments, they mapped them to the genome and assigned them to either transcribed or non-transcribed strand. They observed that only in Mfd deficient mutants (in contrast to UvrD deficient ones) the ratio of repair originating from transcribed (TS) vs non transcribed (NTS) strand is significantly decreased compared to the WT strains [17,19]. Specifically, they observed that the TS/NTS repair ratio decreased overall by a factor of 1.7 in Mfd

deficient cells compared with WT cells, and that the Mfd contribution to TCR was widespread among diverse genes.

However, molecular evidence from multiple *in vitro* and *in vivo* assays has demonstrated that UvrD can also bind to RNAP, promote RNAP backtracking and subsequent towing of RNAP [13]. The binding of UvrD to RNAP has also been confirmed with NMR spectroscopy and non-overlapping surfaces of RNAP were proposed as binding sites for UvrD and Mfd [37]. The extent of UvrD dependent RNAP backtracking was shown to depend on UvrD concentration and may be regulated by anti-backtracking factors, GreA and GreB, or the stress alarmone, ppGpp [13,14]. It was originally hypothesised that UvrD-directed TCR is primarily activated during the SOS-response, whereas steady-state damage is repaired by Mfd-dependent TCR [14]. In a recent report, the same authors updated their UvrD-dependent model of TCR: proposing that a pre-TCR complex, consisting of UvrA and UvrD proteins associated with RNAP continuously, acts as the main NER surveillance complex. They observed a substantial fraction of UvrA and UvrD bound to RNAP before UV exposure and they postulated that Mfd is recruited by stalled pre-TCR complexes, rather than vice versa [15]. This model emphasizes the principal role of transcribing RNAP in all NER and the minor role of Mfd, which participates mostly in removing obstructive RNAPs in front of TCR complexes [15]. By isolating high-molecular-weight genomic DNA isolated from the cell, they confirmed that Rif treatment causes near-absolute inhibition of repair of CPDs [35,11].

Single-molecule imaging studies have provided new insight into NER, such as coupling Mfd dissociation with UvrB loading [38], kinetic details of NER pathway participants [39,40] or about UvrAB-Mfd-RNAP complex dissolution [41]. Here, using single-molecule tracking, we show that UvrA and RNAP protein mobility is strikingly similar in unperturbed cells, consistent with these proteins potentially being complexed in the absence of damage. This was not true for UvrD, demonstrating that the percentage of UvrD present in putative UvrD-RNAP-UvrA complexes is small. Focusing on the number of immobile, DNA-bound molecules, we show that ~8 DNA-bound UvrD-RNAP-UvrA complexes per cell could potentially form in the absence of damage. However, while these complexes may be present our results are not consistent with these being the primary damage sensor for NER.

Our results are consistent with Mfd playing a major role in TCR in *E. coli.* Upon DNA damage, Mfd recruitment to DNA showed no dependency on the presence of UvrA, in agreement with its role upstream of this protein in the Mfd-dependent model of TCR. Inhibiting transcription with Rif abolished Mfd DNA-recruitment following DNA damage, consistent with transcribing RNAPs becoming stalled at DNA lesions being essential for Mfd recruitment to DNA. In contrast, UvrD recruitment to DNA was dependent on the presence of UvrA. Significant recruitment of UvrD to DNA remained when transcription was inhibited with Rif suggesting most activity is independent of actively transcribing RNAP. Furthermore, significant UV-induced DNA recruitment of UvrA and UvrB remained in Rif treated cells. Although our assay measures only protein recruitment to DNA, not on damage repair, this data nevertheless contrasts reports showing that Rif treatment causes near-absolute inhibition of repair of CPDs and therefore, presumably, no recruitment of repair proteins to the damage site. We note that at the Rif concentrations tested, the UV-induced DNA recruitment of UvrD was lower (but

still significant) compared to in untreated cells. Near complete inhibition of repair in previous studies was only observed at very high rifampicin concentrations (750 µg/ml for 60 min) compared to the concentrations used in this study (100 µg/ml for 30 min). It is therefore possible that abolition of UV-induced DNA recruitment for UvrD might occur at higher concentrations. However, our microscopy assay could not be reliably performed with these high Rif doses due to the presence of cell debris associated with cell death, raising the possibility that the lack of CPD repair under these conditions could partly be a consequence of death occurring in a proportion of cells, rather than directly a consequence of transcription inhibition. Importantly, the Rif concentrations used in our study were sufficient to abolish Mfd UV-induced recruitment to DNA despite recruitment of UvrD, UvrA, and UvrB remaining. Together, our live-cell data does not exclude that RNAP backtracking by UvrD may occur during TCR, but shows that most UvrD molecules are recruited to DNA lesions downstream of UvrA, presumably performing their known function in strand displacement [6,14].

Author contributions

Elżbieta Kaja: Conceptualization, Methodology, Investigation, Data curation, Writing - original draft, Writing - Review and Editing; **Donata Vijande**: Conceptualization, Methodology, Investigation, Writing - original draft, Visualisation; **Justyna Kowalczyk**: Conceptualization, Investigation, Validation; **Michał Michalak**: Conceptualization, Investigation, Validation; **Jacek Gapiński**: Supervision, Resources, Methodology; **Carolin Kobras and Philippa Rolfe**: bacterial strain preparation, **Mathew Stracy:** Conceptualization, Methodology, Investigation, Data curation, Writing - original draft, Writing - Review and Editing, Funding acquisition.

Acknowledgements

This work was supported by the National Science Center in Poland (2015/19/P/NZ1/03859), by the Foundation for Polish Science (First TEAM/2016–1/9) and a Wellcome Trust & Royal Society Sir Henry Dale Fellowship (224212/Z/21/Z). For the purpose of Open Access, the author has applied a CC BY public copyright licence to any Author Accepted Manuscript version arising from this submission. The authors would like to thank Paweł Zawadzki for his expertise and assistance throughout all aspects of the study. The authors would like to thank David Sherratt and Stephan Uphoff and their lab members for their technical and methodological support, as well as for sharing bacterial strains.

References

[1] M. Stracy, M. Jaciuk, S. Uphoff, A.N. Kapanidis, M. Nowotny, D.J. Sherratt, P. Zawadzki, Single-molecule imaging of UvrA and UvrB recruitment to DNA lesions in living Escherichia coli, Nat Commun. 7 (2016) 12568. https://doi.org/10.1038/ncomms12568.

[2] J.J. Truglio, D.L. Croteau, B. Van Houten, C. Kisker, Prokaryotic nucleotide excision repair: the UvrABC system, Chem Rev. 106 (2006) 233–252. https://doi.org/10.1021/cr040471u.

[3] A. Sancar, W.D. Rupp, A novel repair enzyme: UVRABC excision nuclease of Escherichia coli cuts a DNA strand on both sides of the damaged region, Cell. 33 (1983) 249–260. https://doi.org/10.1016/0092-8674(83)90354-9.

[4] D.K. Orren, C.P. Selby, J.E. Hearst, A. Sancar, Post-incision steps of nucleotide excision repair in Escherichia coli. Disassembly of the UvrBC-DNA complex by helicase II and DNA polymerase I, J Biol Chem. 267 (1992) 780–788.
[5] C. Kisker, J. Kuper, B. Van Houten, Prokaryotic Nucleotide Excision Repair, Cold Spring Harb Perspect Biol. 5 (2013) a012591. https://doi.org/10.1101/cshperspect.a012591.
[6] C.P. Selby, A. Sancar, Molecular mechanism of transcription-repair coupling, Science. 260 (1993) 53–58. https://doi.org/10.1126/science.8465200.
[7] L.F. Westblade, E.A. Campbell, C. Pukhrambam, J.C. Padovan, B.E. Nickels, V. Lamour, S.A. Darst, Structural basis for the bacterial transcription-repair coupling factor/RNA polymerase interaction, Nucleic Acids Research. 38 (2010) 8357–8369. https://doi.org/10.1093/nar/gkq692.
[8] N. Savery, Prioritizing the repair of DNA damage that is encountered by RNA polymerase, Transcription. 2 (2011) 168–172. https://doi.org/10.4161/trns.2.4.16146.
[9] C.P. Selby, E.M. Witkin, A. Sancar, Escherichia coli mfd mutant deficient in "mutation frequency decline" lacks strand-specific repair: in vitro complementation with purified coupling factor, Proc Natl Acad Sci U S A. 88 (1991) 11574–11578. https://doi.org/10.1073/pnas.88.24.11574.
[10] E.M. Witkin, Radiation-induced mutations and their repair, Science. 152 (1966) 1345–1353. https://doi.org/10.1126/science.152.3727.1345.
[11] K. Howan, J. Monnet, J. Fan, T.R. Strick, Stopped in its tracks: The RNA polymerase molecular motor as a robust sensor of DNA damage, DNA Repair. 20 (2014) 49–57. https://doi.org/10.1016/j.dnarep.2014.02.018.
[12] J.-S. Park, M.T. Marr, J.W. Roberts, E. coli Transcription repair coupling factor (Mfd protein) rescues arrested complexes by promoting forward translocation, Cell. 109 (2002) 757–767. https://doi.org/10.1016/s0092-8674(02)00769-9.
[13] V. Epshtein, V. Kamarthapu, K. McGary, V. Svetlov, B. Ueberheide, S. Proshkin, A. Mironov, E. Nudler, UvrD facilitates DNA repair by pulling RNA polymerase backwards, Nature. 505 (2014) 372–377. https://doi.org/10.1038/nature12928.
[14] V. Epshtein, UvrD helicase: An old dog with a new trick, BioEssays. 37 (2015) 12–19. https://doi.org/10.1002/bies.201400106.
[15] B.K. Bharati, M. Gowder, F. Zheng, K. Alzoubi, V. Svetlov, V. Kamarthapu, J.W. Weaver, V. Epshtein, N. Vasilyev, L. Shen, Y. Zhang, E. Nudler, Crucial role and mechanism of transcription-coupled DNA repair in bacteria, Nature. 604 (2022) 152–159. https://doi.org/10.1038/s41586-022-04530-6.
[16] B. Martinez, B.K. Bharati, V. Epshtein, E. Nudler, Pervasive Transcription-coupled DNA repair in E. coli, Nat Commun. 13 (2022) 1702. https://doi.org/10.1038/s41467-022-28871-y.
[17] O. Adebali, Y.-Y. Chiou, J. Hu, A. Sancar, C.P. Selby, Genome-wide transcription-coupled repair in Escherichia coli is mediated by the Mfd translocase, Proceedings of the National Academy of Sciences. 114 (2017) E2116–E2125. https://doi.org/10.1073/pnas.1700230114.
[18] L.A. Lindsey-Boltz, A. Sancar, The Transcription-Repair Coupling Factor Mfd Prevents and Promotes Mutagenesis in a Context-Dependent Manner, Frontiers in Molecular Biosciences. 8 (2021). https://www.frontiersin.org/articles/10.3389/fmolb.2021.668290 (accessed January 19, 2023).
[19] O. Adebali, A. Sancar, C.P. Selby, Mfd translocase is necessary and sufficient for transcription-coupled repair in Escherichia coli, Journal of Biological Chemistry. 292 (2017) 18386–18391. https://doi.org/10.1074/jbc.C117.818807.
[20] B.J. Bachmann, Pedigrees of some mutant strains of Escherichia coli K-12, Bacteriological Reviews. 36 (1972) 525–557. https://doi.org/10.1128/br.36.4.525-557.1972.
[21] F.V. Subach, G.H. Patterson, S. Manley, J.M. Gillette, J. Lippincott-Schwartz, V.V. Verkhusha, Photoactivatable mCherry for high-resolution two-color fluorescence microscopy, Nat Methods. 6 (2009) 153–159. https://doi.org/10.1038/nmeth.1298.

[22] K.A. Datsenko, B.L. Wanner, One-step inactivation of chromosomal genes in Escherichia coli K-12 using PCR products, Proceedings of the National Academy of Sciences. 97 (2000) 6640–6645. https://doi.org/10.1073/pnas.120163297.
[23] L.C. Thomason, N. Costantino, D.L. Court, E. coli Genome Manipulation by P1 Transduction, Current Protocols in Molecular Biology. 79 (2007) 1.17.1-1.17.8. https://doi.org/10.1002/0471142727.mb0117s79.
[24] M. Stracy, A.J.M. Wollman, E. Kaja, J. Gapinski, J.-E. Lee, V.A. Leek, S.J. McKie, L.A. Mitchenall, A. Maxwell, D.J. Sherratt, M.C. Leake, P. Zawadzki, Single-molecule imaging of DNA gyrase activity in living Escherichia coli, Nucleic Acids Research. 47 (2019) 210–220. https://doi.org/10.1093/nar/gky1143.
[25] O. Sliusarenko, J. Heinritz, T. Emonet, C. Jacobs-Wagner, High-throughput, subpixel precision analysis of bacterial morphogenesis and intracellular spatio-temporal dynamics, Mol Microbiol. 80 (2011) 612–627. https://doi.org/10.1111/j.1365-2958.2011.07579.x.
[26] S. Uphoff, R. Reyes-Lamothe, F. Garza de Leon, D.J. Sherratt, A.N. Kapanidis, Single-molecule DNA repair in live bacteria, Proceedings of the National Academy of Sciences. 110 (2013) 8063–8068. https://doi.org/10.1073/pnas.1301804110.
[27] X. Michalet, A.J. Berglund, Optimal diffusion coefficient estimation in single-particle tracking, Phys Rev E Stat Nonlin Soft Matter Phys. 85 (2012) 061916. https://doi.org/10.1103/PhysRevE.85.061916.
[28] N. Durisic, L. Laparra-Cuervo, A. Sandoval-Álvarez, J.S. Borbely, M. Lakadamyali, Single-molecule evaluation of fluorescent protein photoactivation efficiency using an in vivo nanotemplate, Nat Methods. 11 (2014) 156–162. https://doi.org/10.1038/nmeth.2784.
[29] N.B. Kuemmerle, W.E. Masker, Effect of the uvrD mutation on excision repair, Journal of Bacteriology. 142 (1980) 535–546. https://doi.org/10.1128/jb.142.2.535-546.1980.
[30] M. Stracy, C. Lesterlin, F. Garza de Leon, S. Uphoff, P. Zawadzki, A.N. Kapanidis, Live-cell superresolution microscopy reveals the organization of RNA polymerase in the bacterial nucleoid, Proc Natl Acad Sci U S A. 112 (2015) E4390-4399. https://doi.org/10.1073/pnas.1507592112.
[31] M. Stracy, J. Schweizer, D.J. Sherratt, A.N. Kapanidis, S. Uphoff, C. Lesterlin, Transient non-specific DNA binding dominates the target search of bacterial DNA-binding proteins, Molecular Cell. 81 (2021) 1499-1514.e6. https://doi.org/10.1016/j.molcel.2021.01.039.
[32] M. Wang, C.J. Herrmann, M. Simonovic, D. Szklarczyk, C. von Mering, Version 4.0 of PaxDb: Protein abundance data, integrated across model organisms, tissues, and cell-lines, Proteomics. 15 (2015) 3163–3168. https://doi.org/10.1002/pmic.201400441.
[33] H.M. Arthur, P.B. Eastlake, Transcriptional control of the uvrD gene of Escherichia coli, Gene. 25 (1983) 309–316. https://doi.org/10.1016/0378-1119(83)90235-4.
[34] Y. Taniguchi, P.J. Choi, G.-W. Li, H. Chen, M. Babu, J. Hearn, A. Emili, X.S. Xie, Quantifying E. coli proteome and transcriptome with single-molecule sensitivity in single cells, Science. 329 (2010) 533–538. https://doi.org/10.1126/science.1188308.
[35] H.N. Ho, A.M. van Oijen, H. Ghodke, The transcription-repair coupling factor Mfd associates with RNA polymerase in the absence of exogenous damage, Nat Commun. 9 (2018) 1570. https://doi.org/10.1038/s41467-018-03790-z.
[36] K.S. Lee, H. Balci, H. Jia, T.M. Lohman, T. Ha, Direct imaging of single UvrD helicase dynamics on long single-stranded DNA, Nat Commun. 4 (2013) 1878. https://doi.org/10.1038/ncomms2882.
[37] A.A. Kawale, B.M. Burmann, UvrD helicase–RNA polymerase interactions are governed by UvrD's carboxy-terminal Tudor domain, Commun Biol. 3 (2020) 1–13. https://doi.org/10.1038/s42003-020-01332-2.
[38] H.N. Ho, A.M. van Oijen, H. Ghodke, Single-molecule imaging reveals molecular coupling between transcription and DNA repair machinery in live cells, Nat Commun. 11 (2020) 1478. https://doi.org/10.1038/s41467-020-15182-3.

[39] H. Ghodke, H.N. Ho, A.M. van Oijen, Single-molecule live-cell imaging visualizes parallel pathways of prokaryotic nucleotide excision repair, Nat Commun. 11 (2020) 1477. https://doi.org/10.1038/s41467-020-15179-y.
[40] H. Yokota, Quantitative and kinetic single-molecule analysis of DNA unwinding by *Escherichia coli* UvrD helicase, BIOPHYSICS. 19 (2022) n/a. https://doi.org/10.2142/biophysico.bppb-v19.0006.
[41] J. Fan, M. Leroux-Coyau, N.J. Savery, T.R. Strick, Reconstruction of bacterial transcription-coupled repair at single-molecule resolution, Nature. 536 (2016) 234–237. https://doi.org/10.1038/nature19080.

Supplementary material

Supplementary figures

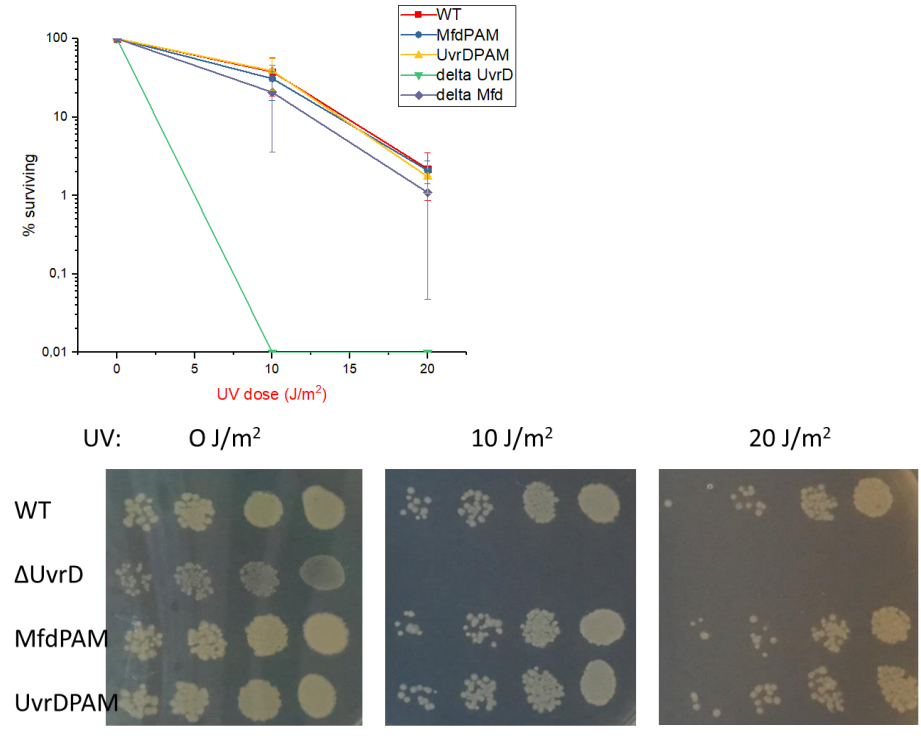

Supplementary figure 1. UV survival assay for WT, MfdPAM, UvrDPAM, ΔuvrD, and Δmfd strains showing that PAmCherry fusions of UvrD and Mfd proteins are fully functional. *Data represent the average percentage survival of three experiments as a function of UV dose (10 and 20 J/m²) (upper panel). Errors represent s.d. of three experimental repeats. The example of plates with no UV (0 J/m²), 10 and 20 J/m² exposure are presented in the lower panel.*

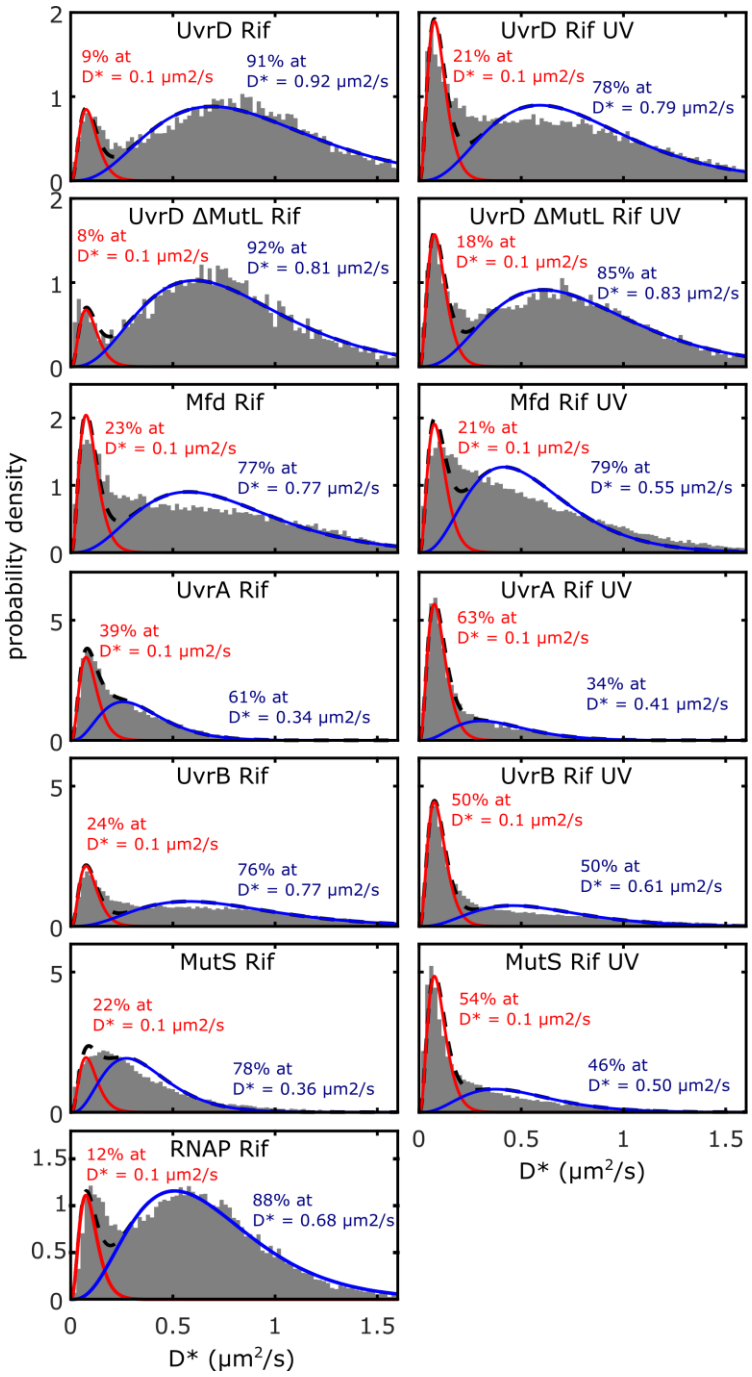

Supplementary figure 2. Protein recruitment to DNA lesions in transcription inhibited cells. *Histograms of single-molecule D* values from tracked PAmCherry fusions to different proteins involved in TCR before (left) and after (right) UV exposure in cells treated with 100 μg/ml rifampicin. Histograms are fitted to a two species model; an immobile population, representing molecules directly or indirectly bound to DNA (constrained fit at D=0.1 μm² s⁻¹), and mobile population, representing molecules diffusing and searching for lesions. Number of trajectories represented in each histogram: UvrD = 11,380; UvrD UV = 27,839; UvrD ΔmutL = 4,561, UvrD ΔmutL UV = 10,941; Mfd = 21,491, Mfd UV = 46,802; UvrA = 13,286; UvrA UV = 7,679; UvrB = 33,394; UvrB UV = 37,704; MutS = 22,270, MutS UV = 31,300; RNAP = 20,854.*

Supplementary tables

Supplementary table 1. Bacterial strains. All strains were constructed in AB1157 original strain.

Strain	Genotype	Source
AB1157	F– , λ– , rac− , thi-1, hisG4, Δ(gpt-proA)62, argE3, thr-1, leuB6, kdgK51, rfbD1, araC14, lacY1, galK2, xylA5, mtl-1, tsx-33, supE44(glnV44), rpsL31(strR), qsr'-0, mgl-51 2	
UvrDPAM	*uvrD:: PAmCherry kan*	This study
MfdPAM	*mfd:: PAmCherry kan*	This study
UvrDPAMΔUvrA	*uvrD:: PAmCherry frt; ΔuvrA kan*	This study
MfdPAMΔUvrA	*mfd:: PAmCherry frt; ΔuvrA kan*	This study
UvrDPAMΔMfd	*uvrD:: PAmCherry frt; Δmfd kan*	This study
MfdPAMΔUvrD	*mfd:: PAmCherry frt; ΔuvrD kan*	This study
UvrDPAMΔMutL	*uvrD:: PAmCherry frt; ΔmutL kan*	This study
UvrAPAM	*UvrA::PAmCherry kan*	Stracy et al, 2016
UvrBPAM	*UvrB::PAmCherry kan*	Stracy et al, 2016
MutSPAM	*MutS:: PAmCherry kan*	Uphoff et al 2016
ΔuvrD	*UvrD deletion kan*	This study
Δmfd	*Mfd deletion kan*	This study
RNAPPAM	*rpoC:: PAmCherry amp (MG1655)*	Endesfelder 2013

Supplementary table 2. Oligonucleotides. Oligonucleotide sequences used for constructing fluorescent fusions.

Name	Sequence
UvrDpamcherryFor	GCCAGGGTATTAAATGGCTGGTGGCGGCATACGCCCGGCTGGAGTCGGTG TCGGCTGGCTCCGCTGCTGGTTC
UvrDpamcherryRev	TGAATGATTTTTTAGGCCAAATAAGGTGCGCAGCACCGCATCCGGCAACGGAGGA TCCCATATGAATATCCTCC
MfdpamcherryFor	AGACGCTGCTCACCCGCTTTGACGGGCAGCGTATAACGATATTGTTCAGGTCGGC TGGCTCCGCTGCTGGTTC
MfdpamcherryRev	ATATGCCCCCATATGTTGAGGCATATCCTAACGAGAATCTGACAACCGTTGAGGAT CCCATATGAATATCCTCC
UvrDdelFor_EK	ATGGACGTTTCTTACCTGCTCGACAGCCTTAATGACAAACAGCGCGAAGCGTAAC CCGGGTGTAGGCTGGAG
UvrDdelRev_EK	TTACACCGACTCCAGCCGGGCGTATGCCGCCACCAGCCATTTAATACCCTGAATA TCCTCCTTAGTTCC
MfddelFor	TTAAGCGATCGCGTTCTCTTCCAGTTCACGCATAAACTGGCGTACCCATTGTAACC CGGGTGTAGGCTGGAG
MfddelRev	ATGCCTGAACAATATCGTTATACGCTGCCCGTCAAAGCGGGTGAGCAGCGGAATA TCCTCCTTAGTTCC
UvrAdelFor	ACCCATAATCTCAAAAACATCAACCTCGTTATCCCCCGCGACAAGCTCATGTAACC CGGGTGTAGGCTGGAG
UvrAdelRev	CTTCGCACTCCGCGACGGTTTCTGGCGTACCGGAGACGAGGATCTCGCCGGAAT ATCCTCCTTAGTTCC

Funding

This work was supported by the National Science Center in Poland (2015/19/P/NZ1/03859), by The Foundation for Polish Science (First TEAM/2016-1/9) and Wellcome Trust grant (224212/Z/21/Z).